

# Synchronization of Interacting Quantum Dipoles

B. Zhu<sup>1</sup>, J. Schachenmayer<sup>1</sup>, M. Xu<sup>1</sup>, F. Herrera<sup>2</sup>, J. G. Restrepo<sup>3</sup>, M. J. Holland<sup>1,\*</sup> and A. M. Rey<sup>1†</sup>

<sup>1</sup>*JILA, NIST, Department of Physics, University of Colorado, 440 UCB, Boulder, CO 80309, USA*

<sup>2</sup>*Department of Physics, Universidad de Santiago de Chile, USACH, Casilla 307 Correo 2 Santiago, Chile and*

<sup>3</sup>*Department of Applied Mathematics, University of Colorado, Boulder, Colorado, 80309, USA*

(Dated: June 17, 2022)

Macroscopic ensembles of radiating dipoles are ubiquitous in the physical and natural sciences. In the classical limit the dipoles can be described as damped-driven oscillators, which are able to spontaneously synchronize and collectively lock their phases. Here we investigate the corresponding phenomenon in the quantum regime with arrays of quantized two-level systems coupled via long-range and anisotropic dipolar interactions. Our calculations demonstrate that the dipoles may overcome the decoherence induced by quantum fluctuations and inhomogeneous couplings and evolve to a synchronized steady-state. This steady-state bears much similarity to that observed in classical systems, and yet also exhibits genuine quantum properties such as quantum correlations and quantum phase diffusion (reminiscent of lasing). Our predictions could be relevant for the development of better atomic clocks and a variety of noise tolerant quantum devices.

PACS numbers: 05.45.Xt, 42.50.Lc, 37.10.Jk, 64.60.Ht

Arrays of synchronized oscillators [1] are ubiquitous in biological [2, 3], physical [4] and engineering [5] systems and are a resource for technological advances [6]. Although there has been significant progress in the study of synchronization in classical systems [7], the understanding of the same phenomena in the quantum realm remains limited. A major obstacle so far is the general problem of the exponential scaling of the Hilbert space with system size which makes calculations dealing with quantum arrays very challenging. In fact, current investigations have been limited to the exact treatment of arrays of a small number of coupled quantum oscillators [8–18], and large ensembles at the mean field level or by including quantum corrections perturbatively [19, 20]. Highly symmetric situations with collective coupling mediated, for example, by a cavity mode [21–25], have also been studied.

Ensembles of radiating dipoles are a natural platform to study quantum synchronization, where coherence can be generated from an incoherent source. One might regard laser systems, where radiation is amplified by the stimulated emission of photons, as a prototypical example. However, lasing is fundamentally a distinct phenomenon from quantum synchronization. This can be seen from the fact that lasing is possible even in the absence of coupling between the atomic dipoles, as is clear in the single atom laser [26], or in atomic beam lasers where only one atom is present in the cavity at any given time. A more relevant situation is the quantum synchronization that takes place in the context of superradiance [27]. It has recently been understood that, in contrast to lasers, steady-state superradiance can produce spectrally pure light [27–29] without stimulated emission. So far this has been demonstrated using a cavity mode as a communication channel that spatially selects an optical mode and enhances the coupling (through the cavity fi-

ness). A more generic and relevant scenario, with great potential and applicability, is the emergence of spontaneous macroscopic quantum synchronization in radiating dipole arrays without a cavity but naturally coupled by the intrinsic anisotropic and long-range dipolar interactions. This is the situation considered in this letter.

We demonstrate that in the presence of an incoherent repumping source, dipole induced cooperative emission can dominate over spatial inhomogeneities and quantum fluctuations and lead to a resilient steady-state exhibiting macroscopic quantum phase coherence and intrinsic quantum correlations. Moreover, the cooperative behavior can be detected by measuring the spectral purity of the emitted radiation. Specifically, the systems we consider are dense arrays of frozen quantum dipoles modeled as quantized two-level systems. By dense arrays of frozen dipoles we mean arrays separated by a distance much closer than the wavelength of the emitted photons and with motional degrees of freedom evolving at a much slower rate than their internal dynamics (Fig. 1). These conditions can be readily satisfied in a variety of quantum systems found in atomic, molecular and optical physics (e.g., Rydberg gases [30–32], alkali vapors [33], alkaline-earth atoms [34], and polar molecules [35]), chemistry (e.g., J-aggregates of dye molecules [36–38]), and biology (e.g., light-harvesting complexes [39, 40]). In cold vapors, one possible way to freeze the motion and tightly trap the particles is via an optical lattice potential (Fig. 1). In this case a sub-optical-wavelength transition must be used in order to reach the tight-packing regime [34, 35].

The dipolar interactions between two dipoles  $a$  and  $b$  with characteristic photon wavelength  $\lambda$  are described by the functions  $g(\mathbf{r}_{ab})$  and  $f(\mathbf{r}_{ab})$ , which depend on the dipoles separation,  $|\mathbf{r}_{ab}|$ , and the angle  $\theta$  between the mean dipole moment and the vector joining the dipoles

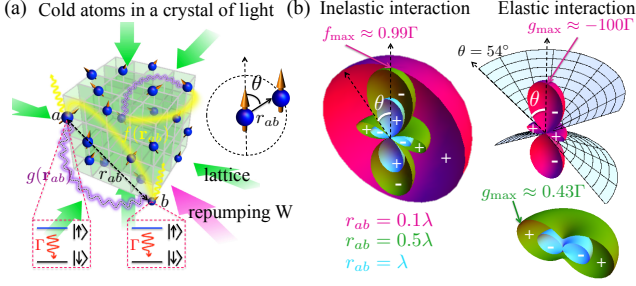


FIG. 1. Arrays of quantum dipoles spontaneously emit and absorb photons at rate  $\Gamma$ . The photons mediate dipolar interactions between dipoles separated by a distance  $\mathbf{r}_{ab}$  with both dissipative,  $f(\mathbf{r}_{ab})$ , and elastic,  $g(\mathbf{r}_{ab})$ , components. A repumping source at a rate  $W$  provides energy to maintain the oscillations and is typically implemented using additional levels. (a) A possible implementation using cold atoms in an optical lattice. (b) The dipolar couplings  $g(\mathbf{r}_{ab})$ , and  $f(\mathbf{r}_{ab})$  exhibit a complex angular distribution as a function of  $\theta$ , the angle between the dipole orientation (determined by an external electromagnetic field) and  $|\mathbf{r}_{ab}|$ . The maximum value of  $f$  and  $g$  for fixed  $|\mathbf{r}_{ab}|$  is denoted as  $f_{\max}$  and  $g_{\max}$ . The cone illustrates the magic angle,  $\theta_m = \arccos(1/\sqrt{3})$ .

[See Fig. 1(a)] [41]:

$$g(\mathbf{r}_{ab}) = -\frac{3\Gamma}{2} \left\{ \sin^2\theta \frac{\cos\zeta_{ab}}{\zeta_{ab}} + (3\cos^2\theta - 1) \left[ \frac{\cos\zeta_{ab}}{(\zeta_{ab})^3} + \frac{\sin\zeta_{ab}}{(\zeta_{ab})^2} \right] \right\}$$

$$f(\mathbf{r}_{ab}) = \frac{3\Gamma}{2} \left\{ \sin^2\theta \frac{\sin\zeta_{ab}}{\zeta_{ab}} + (3\cos^2\theta - 1) \left[ \frac{\sin\zeta_{ab}}{(\zeta_{ab})^3} - \frac{\cos\zeta_{ab}}{(\zeta_{ab})^2} \right] \right\},$$

where  $\zeta_{ab} = 2\pi|\mathbf{r}_{ab}|/\lambda$  and  $\Gamma = f(0)$  is the spontaneous photon emission rate from a single dipole. The function  $g(\mathbf{r}_{ab})$  describes the elastic dipole-dipole and  $f(\mathbf{r}_{ab})$  the inelastic collective photon emission. These terms are similar to those that determine the radiation of classical electric dipoles. The dependence on  $|\mathbf{r}_{ab}|$  describes the propagation of photons from one atom to another. The terms  $\propto 1/|\mathbf{r}_{ab}|$  account for retardation effects in the far-field and those  $\propto 1/|\mathbf{r}_{ab}|^3$  account for instantaneous propagation in the near-field. When  $\zeta_{ab} \ll 1$ , the elastic  $g$  interactions with a strong angular variation are dominant except close to the magic angle  $\theta_m = \arccos(1/\sqrt{3})$ , at which they are greatly suppressed. In contrast, in the near-field  $f(\mathbf{r}_{ab})$  is almost isotropic [see Fig. 1(b)].

The spatially uniform behavior of  $f(\mathbf{r}_{ab})$  at short distance is what gives rise to cooperative effects and superradiant emission [27]. Under generic conditions, however, superradiance is a transient effect and its short duration imposes a limitation to its applicability. To compensate for the fast decay here we add an incoherent repumping driving term at a rate  $W$ . This is needed to generate a synchronized steady state. An incoherent repump is familiar in laser systems where coupling to a third level followed by rapid fluorescence is required to maintain population inversion.

The evolution of  $N$  dipoles is modeled by a quantum

master equation for the reduced density matrix  $\hat{\rho}$  of the dipoles [27]:

$$\frac{d\hat{\rho}}{dt} = -\frac{i}{\hbar} [\hat{H}_0, \hat{\rho}] + \mathcal{L}_f[\hat{\rho}] + \mathcal{L}_W[\hat{\rho}], \quad (1)$$

$$\hat{H}_0 = \frac{\hbar}{2} \sum_{a=1}^N \left[ \delta_a \hat{\sigma}_a^z + \sum_{b=1, b \neq a}^N g(\mathbf{r}_{ab}) \hat{\sigma}_a^+ \hat{\sigma}_b^- \right], \quad (2)$$

$$\mathcal{L}_f[\hat{\rho}] = \frac{1}{2} \sum_{a,b} f(\mathbf{r}_{ab}) (2\hat{\sigma}_b^- \hat{\rho} \hat{\sigma}_a^+ - \hat{\sigma}_a^+ \hat{\sigma}_b^- \hat{\rho} - \hat{\rho} \hat{\sigma}_a^+ \hat{\sigma}_b^-), \quad (3)$$

$$\mathcal{L}_W[\hat{\rho}] = \frac{W}{2} \sum_a (2\hat{\sigma}_a^+ \hat{\rho} \hat{\sigma}_a^- - \hat{\sigma}_a^- \hat{\sigma}_a^+ \hat{\rho} - \hat{\rho} \hat{\sigma}_a^- \hat{\sigma}_a^+). \quad (4)$$

The Hamiltonian  $\hat{H}_0$  generates the coherent evolution of the dipole array where  $\hat{\sigma}_a^{(\pm, z)}$  are the Pauli spin operators for dipole  $a$ ,  $\delta_a$  denotes its bare oscillation frequency and  $\hbar$  is the reduced Planck constant.  $\mathcal{L}_{f,W}$  are operator functionals that describe, respectively, the inelastic photon emission and repumping processes.

Initially, to obtain a qualitative picture and to connect quantum to classical behavior, we perform a mean-field treatment that assumes uncorrelated dipoles, i.e.,  $\hat{\rho} = \bigotimes_a \hat{\rho}_a$ , where each  $\hat{\rho}_a = \sum_{\sigma, \sigma' = \uparrow, \downarrow} \rho_a^{\sigma, \sigma'} |\sigma\rangle \langle \sigma'|$  is a  $2 \times 2$  matrix in the pseudospin 1/2 basis  $\{|\uparrow\rangle, |\downarrow\rangle\}$ . The components of the single-dipole density matrix,  $\hat{\rho}_a$ , can be visualized as a Bloch vector  $\{S_a^\perp(t) \cos \phi_a(t), S_a^\perp(t) \sin \phi_a(t), S_a^z(t)\} = (1/2) \{\rho_a^{\uparrow\downarrow} + \rho_a^{\downarrow\uparrow}, -i(\rho_a^{\uparrow\downarrow} - \rho_a^{\downarrow\uparrow}), \rho_a^{\uparrow\uparrow} - \rho_a^{\downarrow\downarrow}\}$  (Fig. 2). The mean-field solution yields a system of coupled non-linear differential equations for  $\rho_a^{\sigma, \sigma'}$  [41]. In particular the azimuthal phases for each  $a = 1, 2, \dots, N$  evolve as

$$\frac{d\phi_a}{dt} = \delta_a + \sum_{b \neq a=1}^N \frac{S_b^z(t) S_a^\perp(t)}{S_a^\perp(t)} \Re \left[ [g(\mathbf{r}_{ab}) - if(\mathbf{r}_{ab})] e^{i\delta\phi_{ba}} \right] \quad (5)$$

where  $\delta\phi_{ba}(t) = (\phi_b(t) - \phi_a(t))$  and  $\Re$  denotes the real part. The term proportional to  $f(\mathbf{r}_{ab})$  that contains the sine function can be identified with a similar term in the Kuramoto model (KM) [42], the iconic model used to describe classical phase synchronization:  $\dot{\phi}_a(t) = \delta_a + K \sum_b \sin[\delta\phi_{ba}]$ , where  $K$ , the coupling strength per oscillator, must be large enough and positive for synchronization to occur. The term proportional to  $g(\mathbf{r}_{ab})$  that contains the cosine function appears in the Sakaguchi-Kuramoto model [43], a more general but similar synchronization model.

In contrast to the basic KM, the situation here is more complex. This is due to the fact that in Eq. (5) the coupling constants are non-uniform and effectively time-dependent, since  $S_a^\perp(t)$  and  $S_a^z(t)$  are dynamic variables. To investigate whether the mean-field model admits spontaneous synchronization we consider first the simplified case where  $\delta_a = 0$  for all dipoles, impose  $g(\mathbf{r}_{ab}) = 0$  for all pairs, and assume a constant collective decay rate  $Nf(\mathbf{r}_{ab}) \equiv f_{\text{eff}}$  [44]. Fig. 2 shows the

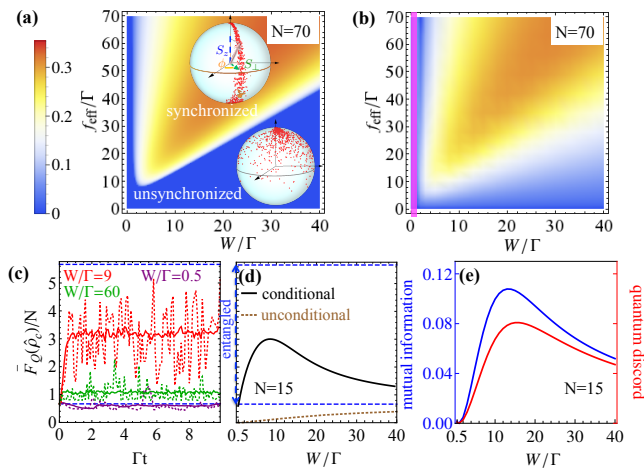


FIG. 2. (a) Mean-field phase diagram calculated from the order parameters  $0 \leq Z \leq 0.5$ . The insets show snapshots of the tips of the Bloch vectors (red points) for dipoles prepared with random initial phases and then evolved to steady-state in both regimes. (b) Quantum phase diagram calculated from  $0 \leq Z_Q \leq 1/\sqrt{8}$ . (c) The time evolution of the conditional QFI exhibits entanglement (dashed line: single trajectory, solid line: mean value of a few trajectories). Panel (d) shows the steady state QFI vs  $W/\Gamma$ . The solid line corresponds to the conditional case. Upon computing the ensemble average one recovers the reduced density matrix which leads to a calculated QFI below the entanglement witness threshold (dashed line). That quantum correlations remain is demonstrated in panel (e) where the correlations in the steady state are quantified by the mutual information  $0 \leq \mathcal{I} \leq 2$  and quantum discord  $0 \leq \mathcal{D} \leq 2$ , shown for  $f_{\text{eff}} = 15\Gamma$ . For all panels,  $\delta_a = g(\mathbf{r}_{ab}) = 0$  and  $f(\mathbf{r}_{ab}) = f_{\text{eff}}/N$ .

phase distribution in the steady-state for an array of oscillators initially prepared with a random distribution of phases for two different values of the repump rate  $W$ . For a slow repumping rate, the system remains unsynchronized. As the repumping rate is increased beyond a threshold value, the system enters a synchronized state, as can be seen by the appearance of phase locking and the resulting narrow phase spread. This can be explained by the fact that one necessary condition for synchronization in the KM is  $K > 0$ , which translates to the requirement  $S_a^z > 0$  on average in our model and thus the need to have sufficiently large repump rate. Regions of synchronization can be quantified by an order parameter  $Z \equiv \frac{1}{N} |\sum_{a=1}^N S_a^z e^{i\phi_a}|$  as shown in Fig. 2(a), which shows the value of  $Z$  obtained from an analytic solution of Eq. (5) [41]. Notice also that at large  $W$  the dipoles are repumped too fast and coherence can not be maintained.

We next proceed to benchmark the validity of the mean-field solution. In the simplified case we consider so far it is possible to exactly solve Eq. (1), the full quantum dynamics, even for many particles. This is due to the invariance of the master equation under individual dipole permutations that reduces the scaling of the Liou-

ville space from exponential,  $4^N$ , to polynomial, of order  $N^3$  [45]. Quantum fluctuations can lead to phase diffusion and to decay of single particle coherences in the steady-state (it is possible for  $\langle \hat{\sigma}_a^+ \rangle \rightarrow 0$  even in a synchronized state), so  $Z$  cannot be used in a beyond mean-field treatment. However, phase locking in quantum mechanics can be quantified by the degree of spin-spin correlations  $Z_Q$ , defined by  $Z_Q^2 \equiv \langle \overline{\hat{\sigma}_a^+ \hat{\sigma}_b^-} \rangle$ , where the bar indicates an average over all pairs of different dipoles  $a$  and  $b$ . For an unsynchronized state  $Z_Q$  is 0 and for a completely synchronized state  $Z_Q$  is  $Z_Q^{\text{max}} = 1/\sqrt{8}$  [28, 29]. The corresponding phase diagram, shown in Fig. 2(b), closely resembles the mean-field one.

A natural question regarding quantum synchronization is whether there is entanglement related to the synchronized state. To determine the non-separability of the steady-state we compute the average of the quantum Fisher information (QFI) and use it as an entanglement witness [41, 46, 47]. Any  $N$  particle state with  $(N^2 + 2N)/3 \geq \bar{F}_Q(\hat{\rho}) > 2N/3$  is entangled (non-separable) and a quantum resource for phase estimation. We first consider a gedanken experiment in which one monitors the system evolution and keeps a record of the emitted photons giving a conditional evolution known as quantum trajectories [48, 49]. In Fig. 2(d) we show calculations of  $\bar{F}_Q(\hat{\rho}_c)$  (with the  $c$  in  $\hat{\rho}_c$  meaning conditional), with  $F_Q(\hat{\rho}_c)$  calculated for individual quantum trajectories and then the averaged. For this conditional evolution we observe entanglement in a parameter regime that correlates with  $Z_Q > 0$  [see Fig. 2(c) and (d)]. However, if we discard the information present in the measurement record, by tracing over the conditional trajectories, and then computing  $F_Q(\hat{\rho})$ , the QFI falls below the entanglement witness threshold [see Fig. 2(d)]. Nevertheless, we find the mixed steady-state contains non-zero quantum correlations in the synchronized regime. This is quantified by the quantum discord  $\mathcal{D}$  [Fig. 2(e)], a type of correlation measure more general than entanglement that differentiates quantum effects from classical ones [50–53]. While there are also classical correlations when  $Z > 0$ , measured by the difference between the mutual information  $\mathcal{I}$  and the  $\mathcal{D}$  [Fig. 2(e)], quantum correlations remain a significant fraction of the total ( $\mathcal{I}$ ) even in the thermodynamic limit [41].

Up to this point we have only considered all-to-all interactions; now we consider the effect of the finite range of the interactions. In the dipole array both  $f(\mathbf{r}_{ab})$  and  $g(\mathbf{r}_{ab})$  are nontrivial functions of  $\mathbf{r}_{ab}$ . To gain insight on how spatial inhomogeneities affect quantum synchronization, we first study a simpler case assuming a power-law cooperative decay  $f(\mathbf{r}_{ab}) \propto |\mathbf{r}_{ab}|^{-\alpha}$ , with the exponent  $\alpha$  as a variable parameter and set both  $g(\mathbf{r}_{ab}) = 0$  and  $\delta_a = 0$ . In the KM with power-law couplings, domains of synchronized oscillators can emerge [54]. Dimensionality plays an important role in finite range interacting systems because it determines the number of nearest-

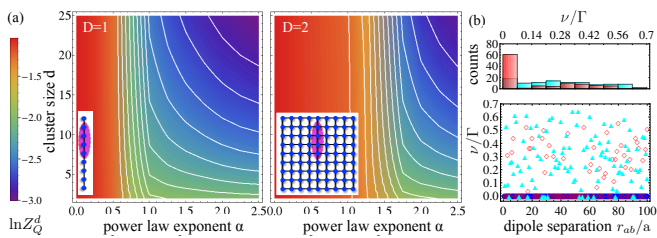


FIG. 3. (a) Spin-spin correlations,  $Z_Q^d$ , in linear clusters containing  $d$  dipoles at optimal repumping  $W$  for power-law couplings  $f(\mathbf{r}_{ab}) = \frac{\Gamma}{4} \left(\frac{a}{r_{ab}}\right)^\alpha$  with lattice spacing  $a$ . We set  $\delta_a = g(\mathbf{r}_{ab}) = 0$  and consider  $N = 900$  dipoles arranged in both linear ( $D = 1$ ) and square lattice ( $D = 2$ ) geometries. Global ( $\alpha \lesssim D/2$ ), partial ( $D/2 \lesssim \alpha \lesssim D$ ) and unsynchronized ( $\alpha \gtrsim D$ ) regimes are observed. Shown are several contour lines (magenta:  $Z_Q^d = 0.14$ ) (b) Pair wise two-time correlation functions in the steady-state are parametrized by  $Z_{a,b}(\tau) = A \cos(\nu\tau) \exp(-\gamma\tau)$  where  $a$  is chosen as the central dipole of a linear chain of  $N = 200$  dipoles. The dipoles are assigned random detunings  $\delta_a$  distributed uniformly in  $[-\Gamma/2, \Gamma/2]$ . The histogram of frequencies  $\nu$  confirms the same synchronization regimes seen in (a).

neighbor connections. To quantify similar phenomena in our system, we compute spin-spin correlations within linear clusters that contain  $d$  dipoles,  $Z_Q^d$ , using a cumulant expansion method [41]. Fig. 3(a) shows these correlations as a function of  $d$  and  $\alpha$  in arrays of dimension  $D = 1$  and 2. For  $\alpha \lesssim D/2$ , global synchronization emerges over an extended region, while for  $D/2 \lesssim \alpha \lesssim D$ , synchronization is local and correlations quickly decrease with cluster size. The magenta contour provides an indicative scale of the synchronized cluster length. For  $\alpha \gtrsim D$  the system is unsynchronized.

An alternative way to characterize domain formation and the fact that it can persist even when there is a variation in the local detunings,  $\delta_a \neq 0$ , is to examine pairwise two-time correlation functions,  $Z_{ab}(\tau) \equiv \lim_{t \rightarrow \infty} \langle (\hat{\sigma}_a^+(t+\tau) + \hat{\sigma}_b^+(t+\tau))(\hat{\sigma}_a^-(t) + \hat{\sigma}_b^-(t)) \rangle$  [Fig. 3(b)]. The oscillations in  $Z_{ab}(\tau)$  encode information about the relative precession rate between different dipoles. Similar synchronization regimes are observed: While for a small  $\alpha$ , dipoles are seen to frequency-lock with the mean detuning frequency (global synchronization), as  $\alpha$  is increased domains begin to form (partial synchronization), and for larger  $\alpha$  a broad distribution of frequencies is observed (no synchronization).

With this foundation in place we now treat the full problem of radiating quantum dipoles incorporating elastic interactions  $g(\mathbf{r}_{ab})$  and the intricate competition of spatially-dependent and anisotropic couplings (both  $g(\mathbf{r}_{ab})$  and  $f(\mathbf{r}_{ab})$  have terms with power law dependence  $\alpha = 1, 2, 3$  on distance) (Fig. 1). We solve the full master equation without any approximation [48] for systems of up to twenty dipoles in a chain using the actual spatial dependence of both  $f(\mathbf{r}_{ab})$  and  $g(\mathbf{r}_{ab})$ , and set  $\delta_a = 0$ .

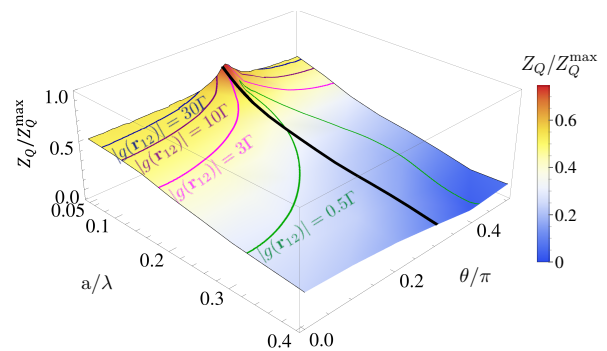


FIG. 4. Synchronization in dipole arrays is demonstrated for twelve dipoles on a line when subjected to incoherent pumping (optimal rate). In this geometry, regardless of the strong angular variation of  $g$  with the lattice spacing  $a$  (see contours) the order parameter,  $Z_Q$ , (normalized by  $Z_Q^{\max} = \sqrt{1/8}$ ) exhibits a weak dependence on  $\theta$  and  $a$  and reaches a maximum at  $\theta = \theta_m$ .

We observe a robust synchronized state that exists in a wide parameter space. In fact we find that the capability for the system to synchronize is determined by  $f_{\text{eff}} \equiv N \overline{f(\mathbf{r}_{ab})}$  as demonstrated by the agreement between the full master equation solution and the much simpler case with constant coupling  $f_{\text{eff}}$  and  $g(\mathbf{r}_{ab}) = 0$  [41]. As long as  $f_{\text{eff}}$  is large enough, we observe that synchronization takes place and is only weakly affected by substantial differences in  $g(\mathbf{r}_{ab})$ , i.e., variations in the dipole array that modify  $g(\mathbf{r}_{ab})$  by two orders of magnitude only decrease the order parameter by a factor of two (Fig. 4). The synchronization can be optimized by tuning the orientation of the dipoles to the magic angle  $\theta_m = \arccos(1/\sqrt{3})$ . For this orientation the order parameter reaches a significant fraction of  $Z_Q^{\max}$ , indicating the emergence of macroscopic spontaneous synchronization of the radiating quantum dipole array.

In summary, we have demonstrated that a system of radiating quantum dipoles can be synchronized in the presence of repumping. The intrinsic macroscopic coherence of the superradiant steady state is inherently resilient to single particle decoherence, spatial inhomogeneities and noisy environmental effects. Potentially this could have relevant application to the development of low-threshold organic lasers, highly efficient solar cells, materials with enhanced chemical reactivity, as well as ultra-precise quantum devices. Moreover, since quantum synchronization is imprinted in the spectral purity of the emitted radiation [29], the generated light may potentially serve as a diagnostic tool of quantum coherences in generic systems beyond cold gases.

*Acknowledgements:* The authors wish to acknowledge useful discussions with David Nesbitt, James K. Thompson, Alexey V. Gorshkov, Emanuel Knill, Kaden R. A. Hazzard, Michael Foss-Feig, Zhe-Xuan Gong, Michael L. Wall, Dominic Meiser and Timur V. Tscherbul. This

work was supported by NIST, the NSF (PIF-1211914 and PFC-1125844), AFOSR, AFOSR-MURI, ARO individual investigator awards, and DARPA QuASAR. Computations utilized the Janus supercomputer, supported by NSF (award number CNS-0821794), NCAR, and CU Boulder/Denver.

- 
- [1] A. Pikovsky, M. Rosenblum, and J. Kurths, *Synchronization: A Universal Concept in Nonlinear Sciences*, Cambridge Nonlinear Science Series (Cambridge University Press, 2003), ISBN 9780521533522.
- [2] S. Yamaguchi, H. Isejima, T. Matsuo, R. Okura, K. Yagita, M. Kobayashi, and H. Okamura, *Science* **302**, 1408 (2003).
- [3] M. Steriade, *Cerebral Cortex* **7**, 583 (1997).
- [4] M. C. Cross, *Phys. Rev. E* **85**, 046214 (2012).
- [5] M. Rohden, A. Sorge, M. Timme, and D. Witthaut, *Phys. Rev. Lett.* **109**, 064101 (2012).
- [6] Q. Li and D. Rus, *Computers*, *IEEE Transactions on* **55**, 214 (2006).
- [7] A. Arenas, A. Diaz-Guilera, J. Kurths, Y. Moreno, and C. Zhou, *Physics Reports* **469**, 93 (2008).
- [8] S. Walter, A. Nunnenkamp, and C. Bruder, *Annalen der Physik* pp. 1521–3889 (2014).
- [9] S.-B. Shim, M. Imboden, and P. Mohanty, *Science* **316**, 95 (2007).
- [10] M. Zhang, G. S. Wiederhecker, S. Manipatruni, A. Barnard, P. McEuen, and M. Lipson, *Phys. Rev. Lett.* **109**, 233906 (2012).
- [11] M. H. Matheny, M. Grau, L. G. Villanueva, R. B. Karabalin, C. Cross, M., and M. L. Roukes, *Phys. Rev. Lett.* **112**, 014101 (2014).
- [12] G. L. Giorgi, F. Galve, G. Manzano, P. Colet, and R. Zambrini, *Phys. Rev. A* **85**, 052101 (2012).
- [13] G. L. Giorgi, F. Plastina, G. Francica, and R. Zambrini, *Phys. Rev. A* **88**, 042115 (2013).
- [14] H. Qiu, B. Julia-Diaz, M. A. Garcia-March, and A. Polls, *Phys. Rev. A* **90**, 033603 (2014).
- [15] M. Xu, D. A. Tieri, E. C. Fine, J. K. Thompson, and M. J. Holland, *Phys. Rev. Lett.* **113**, 154101 (2014).
- [16] V. Ameri, M. Eghbali-Arani, A. Mari, A. Farace, F. Kheirandish, V. Giovannetti, and R. Fazio, arXiv: preprint p. 1412.2585 (2014).
- [17] M. R. Hush, W. Li, S. Genway, I. Lesanovsky, and A. D. Armour, arXiv: preprint p. 1412.1863 (2014).
- [18] S. Walter, A. Nunnenkamp, and C. Bruder, *Phys. Rev. Lett.* **112**, 094102 (2014).
- [19] T. E. Lee, C.-K. Chan, and S. Wang, *Phys. Rev. E* **89**, 022913 (2014).
- [20] T. E. Lee and H. R. Sadeghpour, *Phys. Rev. Lett.* **111**, 234101 (2013).
- [21] G. Heinrich, M. Ludwig, J. Qian, B. Kubala, and F. Marquardt, *Phys. Rev. Lett.* **107**, 043603 (2011).
- [22] M. Ludwig and F. Marquardt, *Phys. Rev. Lett.* **111**, 073603 (2013).
- [23] M. Bagheri, M. Poot, L. Fan, F. Marquardt, and H. X. Tang, *Phys. Rev. Lett.* **111**, 213902 (2013).
- [24] G. Manzano, F. Galve, G. L. Giorgi, E. Hernandez-Garcia, and R. Zambrini, *Sci. Rep.* **3**, 1439 (2013).
- [25] A. Mari, A. Farace, N. Didier, V. Giovannetti, and R. Fazio, *Phys. Rev. Lett.* **111**, 103605 (2013).
- [26] J. McKeever, A. Boca, A. D. Boozer, J. R. Buck, and H. J. Kimble, *Nature* **425**, 268 (2003).
- [27] M. Gross and S. Haroche, *Physics Reports* **93**, 301 (1982).
- [28] J. G. Bohnet, Z. Chen, J. M. Weiner, D. Meiser, M. J. Holland, and J. K. Thompson, *Nature* **484**, 78 (2012).
- [29] D. Meiser and M. J. Holland, *Phys. Rev. A* **81**, 033847 (2010).
- [30] C. van Ditzhuijzen, A. Koenderink, J. Hernández, F. Robicheaux, L. Noordam, and H. van den Heuvell, *Phys. Rev. Lett.* **100**, 243201 (2008).
- [31] K. Afrousheh, P. Bohlouli-Zanjani, D. Vagale, A. Muggford, M. Fedorov, and J. D. D. Martin, *Phys. Rev. Lett.* **93**, 233001 (2004).
- [32] W. R. Anderson, J. R. Veale, and T. F. Gallagher, *Phys. Rev. Lett.* **80**, 249 (1998).
- [33] J. Keaveney, A. Sargsyan, U. Krohn, I. Hughes, D. Sarkisyan, and C. Adams, *Phys. Rev. Lett.* **108**, 173601 (2012).
- [34] B. Olmos, D. Yu, Y. Singh, F. Schreck, K. Bongs, and I. Lesanovsky, *Phys. Rev. Lett.* **110**, 143602 (2013).
- [35] B. Yan, S. A. Moses, B. Gadway, J. P. Covey, K. R. Hazzard, A. M. Rey, D. S. Jin, and J. Ye, *Nature* (2013).
- [36] S. D. Boer and D. A. Wiersma, *Chemical Physics Letters* **165**, 45 (1990).
- [37] S. Ozcelik and D. L. Akins, *Applied Physics Letters* **71**, 3057 (1997).
- [38] F. C. Spano and S. Mukamel, *The Journal of Chemical Physics* **91**, 683 (1989).
- [39] G. Panitchayangkoon, D. Hayes, K. A. Fransted, J. R. Caram, E. Harel, J. Wen, R. E. Blankenship, and G. S. Engel, *Proceedings of the National Academy of Sciences* **107**, 12766 (2010).
- [40] G. D. Scholes, G. R. Fleming, A. Olaya-Castro, and R. van Grondelle, *Nat Chem* **3**, 763 (2014).
- [41] See the Supplemental Material, which includes the details of the analytical and numerical methods used.
- [42] Y. Kuramoto, *Chemical oscillations, waves, and turbulence* (Courier Dover Publications, 2003).
- [43] H. Sakaguchi and Y. Kuramoto, *Progress of Theoretical Physics* **76**, 576 (1986).
- [44] Note: The case of a heterogeneous distribution of  $\delta_a$ 's can be treated at the mean field level [41] and the results are qualitatively similar.
- [45] M. Xu, D. A. Tieri, and M. J. Holland, *Phys. Rev. A* **87**, 062101 (2013).
- [46] H. Strobel, W. Muessel, D. Linnemann, T. Zibold, D. B. Hume, L. Pezz, A. Smerzi, and M. K. Oberthaler, *Science* **345**, 424 (2014).
- [47] P. Hyllus, W. Laskowski, R. Krischek, C. Schwemmer, W. Wieczorek, H. Weinfurter, L. Pezzé, and A. Smerzi, *Phys. Rev. A* **85**, 022321 (2012).
- [48] H. J. Carmichael, *Statistical methods in quantum optics*, vol. 2 (Springer, 1999).
- [49] M. B. Plenio and P. L. Knight, *Rev. Mod. Phys.* **70**, 101 (1998).
- [50] K. Modi, A. Brodutch, H. Cable, T. Paterek, and V. Vedral, *Rev. Mod. Phys.* **84**, 1655 (2012).
- [51] H. Ollivier and W. H. Zurek, *Phys. Rev. Lett.* **88**, 017901 (2001).
- [52] B. Dakić, Y. O. Lipp, X. Ma, M. Ringbauer, S. Kropatschek, S. Barz, T. Paterek, V. Vedral, A. Zeilinger, Č. Brukner, et al., *Nature Physics* **8**, 666

(2012).

- [53] H. Ollivier and W. H. Zurek, Phys. Rev. Lett. **88**, 017901 (2001).  
 [54] N. Uchida, Phys. Rev. Lett. **106**, 064101 (2011).  
 [55] M. Xu and M. Holland, arXiv preprint arXiv:1407.5132 (2014).

- [56] K. Henschel, J. Majer, J. Schmiedmayer, and H. Ritsch, Phys. Rev. A **82**, 033810 (2010).  
 [57] R. Kubo, Journal of the Physical Society of Japan **17**, 1100 (1962).  
 [58] D. O'Dell, S. Giovanazzi, G. Kurizki, and V. M. Akulin, Phys. Rev. Lett. **84**, 5687 (2000).

## Supplemental Material

### Mean-field approach

The mean-field ansatz,  $\hat{\rho} = \bigotimes_a \hat{\rho}_a$ , reduces the dynamics to  $3N$  coupled non-linear differential equations:

$$\begin{aligned} \frac{dS_a^z(t)}{dt} = & -S_a^\perp(t) \sum_{b \neq a} S_b^\perp(t) \left[ f(\mathbf{r}_{ab}) \cos[\phi_b(t) - \phi_a(t)] \right. \\ & \left. - g(\mathbf{r}_{ab}) \sin[\phi_b(t) - \phi_a(t)] \right] - \Gamma \left[ \frac{1}{2} + S_a^z(t) \right] \\ & + W \left[ \frac{1}{2} - S_a^z(t) \right], \end{aligned} \quad (1)$$

$$\begin{aligned} \frac{dS_a^\perp(t)}{dt} = & -S_a^z(t) \sum_{b \neq a} S_b^\perp(t) \left[ g(\mathbf{r}_{ab}) \sin[\phi_b(t) - \phi_a(t)] \right. \\ & \left. - f(\mathbf{r}_{ab}) \cos[\phi_b(t) - \phi_a(t)] \right] - \frac{\Gamma + W}{2} S_a^\perp(t), \end{aligned} \quad (2)$$

along with the previously presented Eq. (3) in the main text. In steady-state, synchronized oscillators possess a collective frequency  $\bar{\omega}$ , and thus a macroscopic phase  $\Phi = \bar{\omega}t$ . We define local order parameters to take into account the effect of the inhomogeneous couplings:

$$X_a e^{i\Phi} = \sum_{b \neq a} f(\mathbf{r}_{ab}) S_b^\perp e^{i\phi_b}, \quad Y_a e^{i\Phi} = \sum_{b \neq a} g(\mathbf{r}_{ab}) S_b^\perp e^{i\phi_b}.$$

Here we consider the case in which the local order parameters vary slowly over the system size, and thus can be regarded as the same for all dipoles. This case includes the all-to-all interactions considered in the main text. This approximation is also found to be good in cases where the range of the interactions is comparable to the system size. Under these conditions, we can write  $X_a \approx f_{\text{eff}} Z$ ,  $Y_a \approx g_{\text{eff}} Z$ , where the global order parameter  $Z$  is defined as  $Z e^{i\Phi} = \frac{1}{N} \sum_a S_a^\perp e^{i\phi_a}$  and the effective couplings are given by  $f_{\text{eff}} = \sum_a \sum_{b \neq a} f(\mathbf{r}_{ab}) / (N-1)$  and  $g_{\text{eff}} = \sum_a \sum_{b \neq a} g(\mathbf{r}_{ab}) / (N-1)$ .

The steady-state solution leads to two self-consistent equations for the order parameter  $Z$  and the collective frequency  $\bar{\omega}$

$$Z = \sum_a^N \frac{ZD[f_{\text{eff}}Q + 2g_{\text{eff}}(\delta_a + \bar{\omega})]}{NQ[4(\delta_a + \bar{\omega})^2 + (2f_{\text{eff}}^2 Z^2 + 2g_{\text{eff}}^2 Z^2 + Q^2)],} \quad (3)$$

$$0 = \sum_a^N \frac{ZD[g_{\text{eff}}Q - 2f_{\text{eff}}(\delta_a + \bar{\omega})]}{NQ[4(\delta_a + \bar{\omega})^2 + (2f_{\text{eff}}^2 Z^2 + 2g_{\text{eff}}^2 Z^2 + Q^2)],} \quad (4)$$

where  $Q = \Gamma + W$  and  $D = W - \Gamma$ . When the dipoles have identical detunings,  $\delta_a = 0$ , the prior equations

reduce to

$$\bar{\omega} = \frac{g_{\text{eff}}Q}{2f_{\text{eff}}}, \quad Z = \frac{\sqrt{f_{\text{eff}}D - Q^2}}{\sqrt{2}f_{\text{eff}}}. \quad (5)$$

The elastic couplings in this limit simply induce a global frequency shift that can be eliminated by moving to a rotating frame. Eq. (5) determines the dependence of  $Z$  on  $W$ . The order parameter  $Z$  reaches a maximum value  $Z_{\text{max}} \approx \sqrt{1/8}$  at  $W_{\text{opt}} \approx f_{\text{eff}}/2$  for  $f_{\text{eff}} \gg 1$ . For this optimal condition, the dipoles radiate with atomic inversion  $S_a^z \approx 1/4$ . This derived inversion is in good agreement with that anticipated for optimal synchronization.

In general, the inclusion of a finite spread  $\Delta$  in  $\delta_a$  decreases the value of the order parameter  $Z$ . For instance, if  $\delta_a$  is sampled from a Lorentzian distribution  $p(\delta_a) = \frac{\Delta}{\pi(\Delta^2 + \delta_a^2)}$ ,

$$Z = \frac{\sqrt{f_{\text{eff}}D - Q^2 + 2\Delta^2 - 2\Delta\sqrt{\Delta^2 + f_{\text{eff}}D}}}{\sqrt{2}f_{\text{eff}}}, \quad (6)$$

and optimal synchronization is obtained at a smaller repumping rate,  $W_{\text{opt}} \approx f_{\text{eff}}/2 - \Delta/\sqrt{2}$ . We note that for given  $f_{\text{eff}}$  and  $W$ , synchronization is destroyed (that is,  $Z = 0$ ) at  $\Delta_c = \frac{Q^2 - f_{\text{eff}}D}{2Q}$ .

### Cumulant expansion approach and two-time correlation between dipoles

The cumulant expansion method is a powerful theoretical tool for including correlation effects beyond the mean-field approximation [29, 55, 56]. We keep two-point correlations such as  $\langle \hat{\sigma}_a^{+, -z} \hat{\sigma}_b^{+, -z} \rangle$ , but factorize three point correlations and higher [57]:

$$\begin{aligned} \langle \hat{\sigma}_a^\alpha \hat{\sigma}_b^\beta \hat{\sigma}_c^\gamma \rangle = & \langle \hat{\sigma}_a^\alpha \hat{\sigma}_b^\beta \rangle \langle \hat{\sigma}_c^\gamma \rangle + \langle \hat{\sigma}_a^\alpha \rangle \langle \hat{\sigma}_b^\beta \hat{\sigma}_c^\gamma \rangle + \langle \hat{\sigma}_a^\alpha \hat{\sigma}_c^\gamma \rangle \langle \hat{\sigma}_b^\beta \rangle \\ & - 2 \langle \hat{\sigma}_a^\alpha \rangle \langle \hat{\sigma}_b^\beta \rangle \langle \hat{\sigma}_c^\gamma \rangle. \end{aligned} \quad (7)$$

This factorization closes the set of dynamical equations of motion for all single particle observables  $\langle \hat{\sigma}_a^{+, -z} \rangle$  and equal-time two-point correlations. Two-time correlation functions can be computed by solving the following equa-

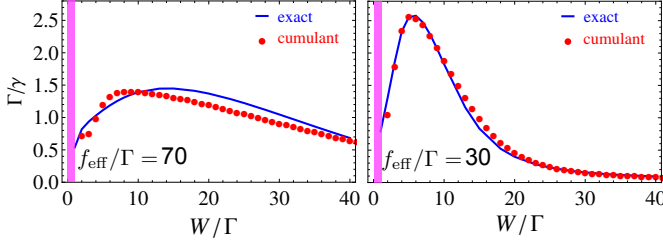


FIG. S1. **Pair-wise two-time correlation functions in the steady-state parametrized by  $Z_{1,2}(\tau) = A \exp(\gamma \tau)$ .** The correlations are calculated for a pair of dipoles in an ensemble of  $N = 70$  dipoles identically coupled with  $f(\mathbf{r}_{ab}) = f_{\text{eff}}/N$ . The cumulant expansion solution agrees with the full calculation except at  $W \ll \Gamma$  where subradiant behavior dominates (purple region) [29].

tion [48]:

$$\begin{aligned} \frac{d\langle \hat{\sigma}_a^+(t+\tau) \hat{\sigma}_b^-(t) \rangle}{d\tau} = & - \left[ i\delta_a + \frac{\Gamma + W}{2} \right] \langle \hat{\sigma}_a^+(t+\tau) \hat{\sigma}_b^-(t) \rangle \\ & + \frac{1}{2} f_{ab} \langle \hat{\sigma}_a^z(t) \rangle \langle \hat{\sigma}_b^+(t+\tau) \hat{\sigma}_b^-(t) \rangle \\ & + \frac{1}{2} \sum_{j \neq a,b} f_{aj} \langle \hat{\sigma}_a^z(t) \rangle \langle \hat{\sigma}_j^+(t+\tau) \hat{\sigma}_b^-(t) \rangle, \end{aligned}$$

where we have approximated  $\langle \hat{\sigma}_a^z(t+\tau) \hat{\sigma}_j^+(t+\tau) \hat{\sigma}_b^-(t) \rangle \approx \langle \hat{\sigma}_a^z(t) \rangle \langle \hat{\sigma}_j^+(t+\tau) \hat{\sigma}_b^-(t) \rangle$ . Comparisons with exact numerical solutions show that the cumulant expansion captures well the steady-state behavior for inhomogeneous couplings  $f(\mathbf{r}_{ab})$ , provided the elastic couplings  $g(\mathbf{r}_{ab})$  are sufficiently small. In Fig. S1 we compute the pair-wise two-time correlation function,  $Z_{ab}(\tau) \equiv \lim_{t \rightarrow \infty} \langle (\hat{\sigma}_a^+(t+\tau) + \hat{\sigma}_b^+(t+\tau)) (\hat{\sigma}_a^-(t) + \hat{\sigma}_b^-(t)) \rangle$ , using both the cumulant expansion and the exact solution. The decay rate of these correlations,  $Z_{ab}(\tau) = A e^{-\tau \gamma}$ , encodes information about the spectral coherence of the emitted radiation. The result shows that  $\Gamma/\gamma$  exhibits the same dependence on  $W/\Gamma$  as  $Z_Q$ .

### Evolution of individual trajectories and quantum Fisher information

The master equation formulation describes the dynamics of the system after a statistical average of many experimental trials. However, the evolution of the system for an individual experimental realization can be quite different. Tracking the evolution of an individual trajectory is equivalent to performing continuous measurements that collect the record of the emitted photons, for example homodyne measurements. The conditional evolution of the system subject to continuous measurements can be modeled by the method of quantum state diffusion [48]. For a single run the state of the system remains pure,  $\hat{\rho}_c = |\psi\rangle\langle\psi|$ , but the average over many trials reduces

the system into a mixed state and recovers the density matrix obtained from the master equation. To probe the entanglement of the dipoles, in Fig. 2 we calculate the average quantum Fisher information for each individual trajectories [46, 47]

$$\bar{F}_Q(\hat{\rho}_c) = \frac{1}{3} (F_Q(\hat{\rho}_c; \hat{J}_x) + F_Q(\hat{\rho}_c; \hat{J}_y) + F_Q(\hat{\rho}_c; \hat{J}_z)),$$

where  $F_Q(\hat{\rho}_c; \hat{\mathcal{H}}) = 4(\langle \psi | \hat{\mathcal{H}}^2 | \psi \rangle - \langle \psi | \hat{\mathcal{H}} | \psi \rangle^2)$ , and  $\hat{J}_{x,y,z}$  are collective angular momentum operators.

### Mutual information and quantum discord

Two systems are correlated if they share information with each other. The total amount of correlation can be quantified by the quantum mutual information  $\mathcal{I} = \mathcal{S}_A + \mathcal{S}_B - \mathcal{S}_{AB}$ , where  $\mathcal{S}_i$  is the von Neumann entropy of the subsystem  $i \in \{A, B, AB\}$  ( $AB$  is the total system spanned by  $A$  and  $B$  together),  $\mathcal{S}_i = -\text{Tr}[\hat{\rho}_i \log_2 \hat{\rho}_i]$ , with  $\hat{\rho}_i$  the reduced density matrix of the subsystem  $i$ . A value varying between 0 and 2 is obtained when  $A$  and  $B$  are pure states or maximally correlated respectively. The mutual information can be separated into a classical and a quantum part. The classical part is  $\mathcal{J}_{B|A} = \max\{\mathcal{S}_B - \mathcal{S}_{B|A}\}$ . Here  $\mathcal{S}_{B|A}$  is the von Neumann entropy of subsystem  $B$  conditioned on the measurement performed on  $A$  and  $\max$  represents maximum value obtainable over all local measurements on  $A$ . The quantum part, known as the quantum discord,  $\mathcal{D}_{B|A} = \mathcal{I} - \mathcal{J}_{B|A}$ , measures the amount of correlations that exceed the classical part and characterizes the ‘‘quantumness’’ of the system [50]. A state with nonzero quantum discord, behaves in a way intrinsically non-classical, since local measurement performed on one of its subsystems can disturb the whole system. In order to calculate  $\mathcal{J}_{B|A}$ , we consider a set of von Neumann measurements  $\hat{\Pi}_{k=1,2}^A = \frac{1}{2}(1 \pm \vec{n}_k \cdot \vec{\sigma}^A)$  with  $|\vec{n}_k|^2 = 1$ , made on the subsystem  $A$  and minimize the corresponding conditional entropy  $\mathcal{S}_{B|A} = \sum_{k=1}^2 \text{Tr}[p_k \mathcal{S}(\hat{\rho}_{B|\Pi_k^A})]$ , where  $p_k = \text{Tr}[\hat{\Pi}_k^A \hat{\rho}]$ ,  $\hat{\rho}_{B|\Pi_k^A} = \text{Tr}_A[\hat{\Pi}_k^A \hat{\rho}] / p_k$  [50]. In Fig. 2(e) we calculate the mutual information from  $\mathcal{I}$  and the quantum discord from  $\mathcal{D}$  using as subsystems  $A$  and  $B$  a pair of dipoles,  $a$  and  $b$  respectively.

### Scaling of mutual information and quantum discord vs particle number

We have shown in the main text that the radiating dipoles exhibit finite classical and quantum correlations in the synchronized steady state via the exact solution of the master equation for a medium size system of  $N = 70$ . To explore these correlations in the thermodynamic limit, we use a cumulant expansion to calculate the quantum

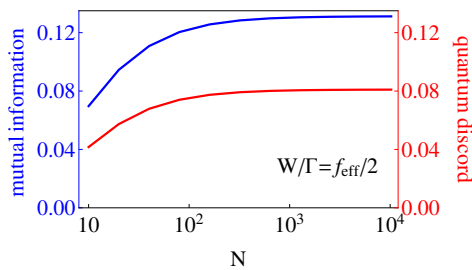


FIG. S2. **Scaling of mutual information and quantum discord vs particle number.** The mutual information  $\mathcal{I}$  and quantum discord  $\mathcal{D}$  at steady state are calculated for different  $N$ , with  $\delta_a = g(\mathbf{r}_{ab}) = 0$  and  $f(\mathbf{r}_{ab}) = f_{\text{eff}}/N$ . The pumping is chosen as  $W/\Gamma = f_{\text{eff}}/2$  so that  $Z_Q > 0$ . Both  $\mathcal{I}$  and  $\mathcal{D}$  increase with system size and stay finite at large  $N$ , indicating the build-up of robust correlations among a large number of synchronized dipoles.

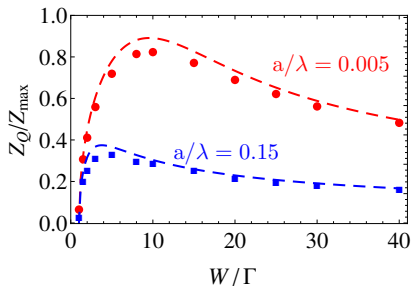


FIG. S3. **Synchronization with dipole-dipole interactions and identical inelastic interactions only.** The order parameter is computed for  $N = 16$  dipoles on a line with  $\theta = \theta_m$  and  $f_{\text{eff}} = \sum_{a,b \neq a} f(\mathbf{r}_{ab})/(N-1)$  (symbols), and for a system with constant  $f(\mathbf{r}_{ab}) = f_{\text{eff}}/N$  and  $g(\mathbf{r}_{ab}) = 0$  (dashed lines). Similar dependence on  $W$  is found for these two different systems. Here the order parameter for dipoles is always smaller in the presence of elastic interactions.

mutual information  $\mathcal{I}$  and discord  $\mathcal{D}$  for increasingly larger systems in Fig. S2. Both  $\mathcal{I}$  and  $\mathcal{D}$  increase until reaching a finite value independent of the system size, showing the coexistence of classical and quantum correlations in a macroscopic system of dipoles when they are synchronized.

### Inelastic interactions and the capability of synchronization

The mean-field approach shows that the total inelastic interaction  $f_{\text{eff}}$  is responsible for the synchronization, although each pair of dipoles can be coupled by different  $f(\mathbf{r}_{ab})$ . In Fig. S3, we solve the master equation Eq. (2) exactly for coupled dipoles arranged in a 1D chain, and for an array of identically coupled dipoles with the same  $f_{\text{eff}}$  but experiencing only inelastic interactions. The calculated order parameters agree well with each other, showing that the capability of the dipole system to synchronize can be characterized by the quantity  $f_{\text{eff}}$ , in spite of the complex geometry of the dipolar interactions. The elastic interaction, on the contrary, is responsible for the decrease of the order parameter and tends to desynchronize the dipoles. For optimal synchronization, one may suppress the elastic interactions either by choosing the magic polarization angle or by using a spatial configuration of external fields which enforces the “averaging out” of the dominant elastic interactions [58].